

Measurement of the B^+ production cross section in $p\bar{p}$ collisions at $\sqrt{s} = 1960$ GeV

A. Abulencia,²⁴ J. Adelman,¹³ T. Affolder,¹⁰ T. Akimoto,⁵⁶ M. G. Albrow,¹⁷ D. Ambrose,¹⁷ S. Amerio,⁴⁴ D. Amidei,³⁵
A. Anastassov,⁵³ K. Anikeev,¹⁷ A. Annovi,¹⁹ J. Antos,¹⁴ M. Aoki,⁵⁶ G. Apollinari,¹⁷ J.-F. Arguin,³⁴ T. Arisawa,⁵⁸
A. Artikov,¹⁵ W. Ashmanskas,¹⁷ A. Attal,⁸ F. Azfar,⁴³ P. Azzi-Bacchetta,⁴⁴ P. Azzurri,⁴⁷ N. Bacchetta,⁴⁴ W. Badgett,¹⁷
A. Barbaro-Galtieri,²⁹ V. E. Barnes,⁴⁹ B. A. Barnett,²⁵ S. Baroiant,⁷ V. Bartsch,³¹ G. Bauer,³³ F. Bedeschi,⁴⁷ S. Behari,²⁵
S. Belforte,⁵⁵ G. Bellettini,⁴⁷ J. Bellinger,⁶⁰ A. Belloni,³³ D. Benjamin,¹⁶ A. Beretvas,¹⁷ J. Beringer,²⁹ T. Berry,³⁰
A. Bhatti,⁵¹ M. Binkley,¹⁷ D. Bisello,⁴⁴ R. E. Blair,² C. Blocker,⁶ B. Blumenfeld,²⁵ A. Bocci,¹⁶ A. Bodek,⁵⁰ V. Boisvert,⁵⁰
G. Bolla,⁴⁹ A. Bolshov,³³ D. Bortoletto,⁴⁹ J. Boudreau,⁴⁸ A. Boveia,¹⁰ B. Brau,¹⁰ L. Brigliadori,⁵ C. Bromberg,³⁶
E. Brubaker,¹³ J. Budagov,¹⁵ H. S. Budd,⁵⁰ S. Budd,²⁴ S. Budroni,⁴⁷ K. Burkett,¹⁷ G. Busetto,⁴⁴ P. Bussey,²¹ K. L. Byrum,²
S. Cabrera,^{16,o} M. Campanelli,²⁰ M. Campbell,³⁵ F. Canelli,¹⁷ A. Canepa,⁴⁹ S. Carillo,^{18,i} D. Carlsmith,⁶⁰ R. Carosi,⁴⁷
M. Casarsa,⁵⁵ A. Castro,⁵ P. Catastini,⁴⁷ D. Cauz,⁵⁵ M. Cavalli-Sforza,³ A. Cerri,²⁹ L. Cerrito,^{43,m} S. H. Chang,²⁸
Y. C. Chen,¹ M. Chertok,⁷ G. Chiarelli,⁴⁷ G. Chlachidze,¹⁵ F. Chlebana,¹⁷ I. Cho,²⁸ K. Cho,²⁸ D. Chokheli,¹⁵ J. P. Chou,²²
G. Choudalakis,³³ S. H. Chuang,⁶⁰ K. Chung,¹² W. H. Chung,⁶⁰ Y. S. Chung,⁵⁰ M. Ciljak,⁴⁷ C. I. Ciobanu,²⁴ M. A. Ciocci,⁴⁷
A. Clark,²⁰ D. Clark,⁶ M. Coca,¹⁶ G. Compostella,⁴⁴ M. E. Convery,⁵¹ J. Conway,⁷ B. Cooper,³⁶ K. Copic,³⁵ M. Cordelli,¹⁹
G. Cortiana,⁴⁴ F. Crescioli,⁴⁷ C. Cuenca Almenar,⁷ J. Cuevas,^{11,l} R. Culbertson,¹⁷ J. C. Cully,³⁵ D. Cyr,⁶⁰ S. DaRonco,⁴⁴
M. Datta,¹⁷ S. D'Auria,²¹ T. Davies,²¹ M. D'Onofrio,³ D. Dagenhart,⁶ P. de Barbaro,⁵⁰ S. De Cecco,⁵² A. Deisher,²⁹
G. De Lentdecker,^{50,c} M. Dell'Orso,⁴⁷ F. Delli Paoli,⁴⁴ L. Demortier,⁵¹ J. Deng,¹⁶ M. Deninno,⁵ D. De Pedis,⁵²
P. F. Derwent,¹⁷ G. P. Di Giovanni,⁴⁵ C. Dionisi,⁵² B. Di Ruzza,⁵⁵ J. R. Dittmann,⁴ P. DiTuro,⁵³ C. Dörr,²⁶ S. Donati,⁴⁷
M. Donega,²⁰ P. Dong,⁸ J. Donini,⁴⁴ T. Dorigo,⁴⁴ S. Dube,⁵³ J. Efron,⁴⁰ R. Erbacher,⁷ D. Errede,²⁴ S. Errede,²⁴ R. Eusebi,¹⁷
H. C. Fang,²⁹ S. Farrington,³⁰ I. Fedorko,⁴⁷ W. T. Fedorko,¹³ R. G. Feild,⁶¹ M. Feindt,²⁶ J. P. Fernandez,³² R. Field,¹⁸
G. Flanagan,⁴⁹ A. Foland,²² S. Forrester,⁷ G. W. Foster,¹⁷ M. Franklin,²² J. C. Freeman,²⁹ I. Furic,¹³ M. Gallinaro,⁵¹
J. Galyardt,¹² J. E. Garcia,⁴⁷ F. Garberon,¹⁰ A. F. Garfinkel,⁴⁹ C. Gay,⁶¹ H. Gerberich,²⁴ D. Gerdes,³⁵ S. Giagu,⁵²
P. Giannetti,⁴⁷ A. Gibson,²⁹ K. Gibson,⁴⁸ J. L. Gimmell,⁵⁰ C. Ginsburg,¹⁷ N. Giokaris,^{15,a} M. Giordani,⁵⁵ P. Giromini,¹⁹
M. Giunta,⁴⁷ G. Giurgiu,¹² V. Glagolev,¹⁵ D. Glenzinski,¹⁷ M. Gold,³⁸ N. Goldschmidt,¹⁸ J. Goldstein,^{43,b} A. Golossanov,¹⁷
G. Gomez,¹¹ G. Gomez-Ceballos,¹¹ M. Goncharov,⁵⁴ O. González,³² I. Gorelov,³⁸ A. T. Goshaw,¹⁶ K. Goulianos,⁵¹
A. Gresele,⁴⁴ M. Griffiths,³⁰ S. Grinstein,²² C. Grosso-Pilcher,¹³ R. C. Group,¹⁸ U. Grundler,²⁴ J. Guimaraes da Costa,²²
Z. Gunay-Unalan,³⁶ C. Haber,²⁹ K. Hahn,³³ S. R. Hahn,¹⁷ E. Halkiadakis,⁵³ A. Hamilton,³⁴ B.-Y. Han,⁵⁰ J. Y. Han,⁵⁰
R. Handler,⁶⁰ F. Happacher,¹⁹ K. Hara,⁵⁶ M. Hare,⁵⁷ S. Harper,⁴³ R. F. Harr,⁵⁹ R. M. Harris,¹⁷ M. Hartz,⁴⁸
K. Hatakeyama,⁵¹ J. Hauser,⁸ A. Heijboer,⁴⁶ B. Heinemann,³⁰ J. Heinrich,⁴⁶ C. Henderson,³³ M. Herndon,⁶⁰ J. Heuser,²⁶
D. Hidas,¹⁶ C. S. Hill,^{10,b} D. Hirschbuehl,²⁶ A. Hocker,¹⁷ A. Holloway,²² S. Hou,¹ M. Houlden,³⁰ S.-C. Hsu,⁹
B. T. Huffman,⁴³ R. E. Hughes,⁴⁰ U. Husemann,⁶¹ J. Huston,³⁶ J. Incandela,¹⁰ G. Introzzi,⁴⁷ M. Iori,⁵² Y. Ishizawa,⁵⁶
A. Ivanov,⁷ B. Iyutin,³³ E. James,¹⁷ D. Jang,⁵³ B. Jayatilaka,³⁵ D. Jeans,⁵² H. Jensen,¹⁷ E. J. Jeon,²⁸ S. Jindariani,¹⁸
M. Jones,⁴⁹ K. K. Joo,²⁸ S. Y. Jun,¹² J. E. Jung,²⁸ T. R. Junk,²⁴ T. Kamon,⁵⁴ P. E. Karchin,⁵⁹ Y. Kato,⁴² Y. Kemp,²⁶
R. Kephart,¹⁷ U. Kerzel,²⁶ V. Khotilovich,⁵⁴ B. Kilminster,⁴⁰ D. H. Kim,²⁸ H. S. Kim,²⁸ J. E. Kim,²⁸ M. J. Kim,¹²
S. B. Kim,²⁸ S. H. Kim,⁵⁶ Y. K. Kim,¹³ N. Kimura,⁵⁶ L. Kirsch,⁶ S. Klimentenko,¹⁸ M. Klute,³³ B. Knuteson,³³ B. R. Ko,¹⁶
K. Kondo,⁵⁸ D. J. Kong,²⁸ J. Konigsberg,¹⁸ A. Korytov,¹⁸ A. V. Kotwal,¹⁶ A. Kovalev,⁴⁶ A. C. Kraan,⁴⁶ J. Kraus,²⁴
I. Kravchenko,³³ M. Kreps,²⁶ J. Kroll,⁴⁶ N. Krumnack,⁴ M. Kruse,¹⁶ V. Krutelyov,¹⁰ T. Kubo,⁵⁶ S. E. Kuhlmann,²
T. Kuhr,²⁶ Y. Kusakabe,⁵⁸ S. Kwang,¹³ A. T. Laasanen,⁴⁹ S. Lai,³⁴ S. Lami,⁴⁷ S. Lammel,¹⁷ M. Lancaster,³¹ R. L. Lander,⁷
K. Lannon,⁴⁰ A. Lath,⁵³ G. Latino,⁴⁷ I. Lazzizzera,⁴⁴ T. LeCompte,² J. Lee,⁵⁰ J. Lee,²⁸ Y. J. Lee,²⁸ S. W. Lee,^{54,n}
R. Lefèvre,³ N. Leonardo,³³ S. Leone,⁴⁷ S. Levy,¹³ J. D. Lewis,¹⁷ C. Lin,⁶¹ C. S. Lin,¹⁷ M. Lindgren,¹⁷ E. Lipeles,⁹
A. Lister,⁷ D. O. Litvintsev,¹⁷ T. Liu,¹⁷ N. S. Lockyer,⁴⁶ A. Loginov,⁶¹ M. Loreti,⁴⁴ P. Loverre,⁵² R.-S. Lu,¹ D. Lucchesi,⁴⁴
P. Lujan,²⁹ P. Lukens,¹⁷ G. Lungu,¹⁸ L. Lyons,⁴³ J. Lys,²⁹ R. Lysak,¹⁴ E. Lytken,⁴⁹ P. Mack,²⁶ D. MacQueen,³⁴
R. Madrak,¹⁷ K. Maeshima,¹⁷ K. Makhoul,³³ T. Maki,²³ P. Maksimovic,²⁵ S. Malde,⁴³ G. Manca,³⁰ F. Margaroli,⁵
R. Marginean,¹⁷ C. Marino,²⁶ C. P. Marino,²⁴ A. Martin,⁶¹ M. Martin,²¹ V. Martin,^{21,g} M. Martínez,³ T. Maruyama,⁵⁶
P. Mastrandrea,⁵² T. Masubuchi,⁵⁶ H. Matsunaga,⁵⁶ M. E. Mattson,⁵⁹ R. Mazini,³⁴ P. Mazzanti,⁵ K. S. McFarland,⁵⁰
P. McIntyre,⁵⁴ R. McNulty,^{30,f} A. Mehta,³⁰ P. Mehtala,²³ S. Menzemer,^{11,h} A. Menzione,⁴⁷ P. Merkel,⁴⁹ C. Mesropian,⁵¹
A. Messina,³⁶ T. Miao,¹⁷ N. Miladinovic,⁶ J. Miles,³³ R. Miller,³⁶ C. Mills,¹⁰ M. Milnik,²⁶ A. Mitra,¹ G. Mitselmakher,¹⁸
A. Miyamoto,²⁷ S. Moed,²⁰ N. Moggi,⁵ B. Mohr,⁸ R. Moore,¹⁷ M. Morello,⁴⁷ P. Movilla Fernandez,²⁹ J. Mülmenstädt,²⁹
A. Mukherjee,¹⁷ Th. Muller,²⁶ R. Mumford,²⁵ P. Murat,¹⁷ J. Nachtman,¹⁷ A. Nagano,⁵⁶ J. Naganoma,⁵⁸ I. Nakano,⁴¹
A. Napier,⁵⁷ V. Necula,¹⁸ C. Neu,⁴⁶ M. S. Neubauer,⁹ J. Nielsen,²⁹ T. Nigmanov,⁴⁸ L. Nodulman,² O. Norniella,³

E. Nurse,³¹ S. H. Oh,¹⁶ Y. D. Oh,²⁸ I. Oksuzian,¹⁸ T. Okusawa,⁴² R. Oldeman,³⁰ R. Orava,²³ K. Osterberg,²³ C. Pagliarone,⁴⁷ E. Palencia,¹¹ V. Papadimitriou,¹⁷ A. A. Paramonov,¹³ B. Parks,⁴⁰ S. Pashapour,³⁴ J. Patrick,¹⁷ G. Pauletta,⁵⁵ M. Paulini,¹² C. Paus,³³ D. E. Pellett,⁷ A. Penzo,⁵⁵ T. J. Phillips,¹⁶ G. Piacentino,⁴⁷ J. Piedra,⁴⁵ L. Pinera,¹⁸ K. Pitts,²⁴ C. Plager,⁸ L. Pondrom,⁶⁰ X. Portell,³ O. Poukhov,¹⁵ N. Pounder,⁴³ F. Prakoshyn,¹⁵ A. Pronko,¹⁷ J. Proudfoot,² F. Ptohos,^{19,e} G. Punzi,⁴⁷ J. Pursley,²⁵ J. Rademacker,^{43,b} A. Rahaman,⁴⁸ N. Ranjan,⁴⁹ S. Rappoccio,²² B. Reisert,¹⁷ V. Rekovic,³⁸ P. Renton,⁴³ M. Rescigno,⁵² S. Richter,²⁶ F. Rimondi,⁵ L. Ristori,⁴⁷ A. Robson,²¹ T. Rodrigo,¹¹ E. Rogers,²⁴ S. Rolli,⁵⁷ R. Roser,¹⁷ M. Rossi,⁵⁵ R. Rossin,¹⁸ A. Ruiz,¹¹ J. Russ,¹² V. Rusu,¹³ H. Saarikko,²³ S. Sabik,³⁴ A. Safonov,⁵⁴ W. K. Sakumoto,⁵⁰ G. Salamanna,⁵² O. Saltó,³ D. Saltzberg,⁸ C. Sánchez,³ L. Santi,⁵⁵ S. Sarkar,⁵² L. Sartori,⁴⁷ K. Sato,¹⁷ P. Savard,³⁴ A. Savoy-Navarro,⁴⁵ T. Scheidle,²⁶ P. Schlabach,¹⁷ E. E. Schmidt,¹⁷ M. P. Schmidt,⁶¹ M. Schmitt,³⁹ T. Schwarz,⁷ L. Scodellaro,¹¹ A. L. Scott,¹⁰ A. Scribano,⁴⁷ F. Scuri,⁴⁷ A. Sedov,⁴⁹ S. Seidel,³⁸ Y. Seiya,⁴² A. Semenov,¹⁵ L. Sexton-Kennedy,¹⁷ A. Sfyrla,²⁰ M. D. Shapiro,²⁹ T. Shears,³⁰ P. F. Shepard,⁴⁸ D. Sherman,²² M. Shimojima,^{56,k} M. Shochet,¹³ Y. Shon,⁶⁰ I. Shreyber,³⁷ A. Sidoti,⁴⁷ P. Sinervo,³⁴ A. Sisakyan,¹⁵ J. Sjolin,⁴³ A. J. Slaughter,¹⁷ J. Slaunwhite,⁴⁰ K. Sliwa,⁵⁷ J. R. Smith,⁷ F. D. Snider,¹⁷ R. Snihur,³⁴ M. Soderberg,³⁵ A. Soha,⁷ S. Somalwar,⁵³ V. Sorin,³⁶ J. Spalding,¹⁷ F. Spinella,⁴⁷ T. Spreitzer,³⁴ P. Squillacioti,⁴⁷ M. Stanitzki,⁶¹ A. Staveris-Polykalas,⁴⁷ R. St. Denis,²¹ B. Stelzer,⁸ O. Stelzer-Chilton,⁴³ D. Stentz,³⁹ J. Strologas,³⁸ D. Stuart,¹⁰ J. S. Suh,²⁸ A. Sukhanov,¹⁸ H. Sun,⁵⁷ T. Suzuki,⁵⁶ A. Taffard,²⁴ R. Takashima,⁴¹ Y. Takeuchi,⁵⁶ K. Takikawa,⁵⁶ M. Tanaka,² R. Tanaka,⁴¹ M. Tecchio,³⁵ P. K. Teng,¹ K. Terashi,⁵¹ J. Thom,^{17,d} A. S. Thompson,²¹ E. Thomson,⁴⁶ P. Tipton,⁶¹ V. Tiwari,¹² S. Tkaczyk,¹⁷ D. Toback,⁵⁴ S. Tokar,¹⁴ K. Tollefson,³⁶ T. Tomura,⁵⁶ D. Tonelli,⁴⁷ S. Torre,¹⁹ D. Torretta,¹⁷ S. Tourneur,⁴⁵ W. Trischuk,³⁴ R. Tsuchiya,⁵⁸ S. Tsuno,⁴¹ N. Turini,⁴⁷ F. Ukegawa,⁵⁶ T. Unverhau,²¹ S. Uozumi,⁵⁶ D. Usynin,⁴⁶ S. Vallecorsa,²⁰ N. van Remortel,²³ A. Varganov,³⁵ E. Vataha,³⁸ F. Vázquez,^{18,i} G. Velez,¹⁷ G. Veramendi,²⁴ V. Veszpremi,⁴⁹ R. Vidal,¹⁷ I. Vila,¹¹ R. Vilar,¹¹ T. Vine,³¹ I. Vollrath,³⁴ I. Volobouev,^{29,n} G. Volpi,⁴⁷ F. Würthwein,⁹ P. Wagner,⁵⁴ R. G. Wagner,² R. L. Wagner,¹⁷ J. Wagner,²⁶ W. Wagner,²⁶ R. Wallny,⁸ S. M. Wang,¹ A. Warburton,³⁴ S. Waschke,²¹ D. Waters,³¹ B. Whitehouse,⁵⁷ D. Whiteson,⁴⁶ A. B. Wicklund,² E. Wicklund,¹⁷ G. Williams,³⁴ H. H. Williams,⁴⁶ P. Wilson,¹⁷ B. L. Winer,⁴⁰ P. Wittich,^{17,d} S. Wolbers,¹⁷ C. Wolfe,¹³ T. Wright,³⁵ X. Wu,²⁰ S. M. Wynne,³⁰ A. Yagil,¹⁷ K. Yamamoto,⁴² J. Yamaoka,⁵³ T. Yamashita,⁴¹ C. Yang,⁶¹ U. K. Yang,^{13,j} Y. C. Yang,²⁸ W. M. Yao,²⁹ G. P. Yeh,¹⁷ J. Yoh,¹⁷ K. Yorita,¹³ T. Yoshida,⁴² G. B. Yu,⁵⁰ I. Yu,²⁸ S. S. Yu,¹⁷ J. C. Yun,¹⁷ L. Zanello,⁵² A. Zanetti,⁵⁵ I. Zaw,²² X. Zhang,²⁴ J. Zhou,⁵³ and S. Zucchelli⁵

(CDF Collaboration)

¹*Institute of Physics, Academia Sinica, Taipei, Taiwan 11529, People's Republic of China*²*Argonne National Laboratory, Argonne, Illinois 60439, USA*³*Institut de Física d'Altes Energies, Universitat Autònoma de Barcelona, E-08193, Bellaterra (Barcelona), Spain*⁴*Baylor University, Waco, Texas 76798, USA*⁵*Istituto Nazionale di Fisica Nucleare, University of Bologna, I-40127 Bologna, Italy*⁶*Brandeis University, Waltham, Massachusetts 02254, USA*⁷*University of California, Davis, Davis, California 95616, USA*⁸*University of California, Los Angeles, Los Angeles, California 90024, USA*⁹*University of California, San Diego, La Jolla, California 92093, USA*¹⁰*University of California, Santa Barbara, Santa Barbara, California 93106, USA*¹¹*Instituto de Física de Cantabria, CSIC-University of Cantabria, 39005 Santander, Spain*¹²*Carnegie Mellon University, Pittsburgh, Pennsylvania 15213, USA*¹³*Enrico Fermi Institute, University of Chicago, Chicago, Illinois 60637, USA*¹⁴*Comenius University, 842 48 Bratislava, Slovakia; Institute of Experimental Physics, 040 01 Kosice, Slovakia*¹⁵*Joint Institute for Nuclear Research, RU-141980 Dubna, Russia*¹⁶*Duke University, Durham, North Carolina 27708*¹⁷*Fermi National Accelerator Laboratory, Batavia, Illinois 60510, USA*¹⁸*University of Florida, Gainesville, Florida 32611, USA*¹⁹*Laboratori Nazionali di Frascati, Istituto Nazionale di Fisica Nucleare, I-00044 Frascati, Italy*²⁰*University of Geneva, CH-1211 Geneva 4, Switzerland*²¹*Glasgow University, Glasgow G12 8QQ, United Kingdom*²²*Harvard University, Cambridge, Massachusetts 02138, USA*²³*Division of High Energy Physics, Department of Physics, University of Helsinki and Helsinki Institute of Physics, FIN-00014, Helsinki, Finland*²⁴*University of Illinois, Urbana, Illinois 61801, USA*²⁵*The Johns Hopkins University, Baltimore, Maryland 21218, USA*²⁶*Institut für Experimentelle Kernphysik, Universität Karlsruhe, 76128 Karlsruhe, Germany*

- ²⁷High Energy Accelerator Research Organization (KEK), Tsukuba, Ibaraki 305, Japan
²⁸Center for High Energy Physics: Kyungpook National University, Taegu 702-701, Korea;
 Seoul National University, Seoul 151-742, Korea; and SungKyunKwan University, Suwon 440-746, Korea
²⁹Ernest Orlando Lawrence Berkeley National Laboratory, Berkeley, California 94720, USA
³⁰University of Liverpool, Liverpool L69 7ZE, United Kingdom
³¹University College London, London WC1E 6BT, United Kingdom
³²Centro de Investigaciones Energeticas Medioambientales y Tecnologicas, E-28040 Madrid, Spain
³³Massachusetts Institute of Technology, Cambridge, Massachusetts 02139, USA
³⁴Institute of Particle Physics: McGill University, Montréal, Canada H3A 2T8; and University of Toronto, Toronto, Canada M5S 1A7
³⁵University of Michigan, Ann Arbor, Michigan 48109, USA
³⁶Michigan State University, East Lansing, Michigan 48824, USA
³⁷Institution for Theoretical and Experimental Physics, ITEP, Moscow 117259, Russia
³⁸University of New Mexico, Albuquerque, New Mexico 87131, USA
³⁹Northwestern University, Evanston, Illinois 60208, USA
⁴⁰The Ohio State University, Columbus, Ohio 43210, USA
⁴¹Okayama University, Okayama 700-8530, Japan
⁴²Osaka City University, Osaka 588, Japan
⁴³University of Oxford, Oxford OX1 3RH, United Kingdom
⁴⁴University of Padova, Istituto Nazionale di Fisica Nucleare, Sezione di Padova-Trento, I-35131 Padova, Italy
⁴⁵LPNHE, Université Pierre et Marie Curie/IN2P3-CNRS, UMR7585, Paris, F-75252 France
⁴⁶University of Pennsylvania, Philadelphia, Pennsylvania 19104, USA
⁴⁷Istituto Nazionale di Fisica Nucleare Pisa, Universities of Pisa, Siena and Scuola Normale Superiore, I-56127 Pisa, Italy
⁴⁸University of Pittsburgh, Pittsburgh, Pennsylvania 15260, USA
⁴⁹Purdue University, West Lafayette, Indiana 47907, USA
⁵⁰University of Rochester, Rochester, New York 14627, USA
⁵¹The Rockefeller University, New York, New York 10021, USA
⁵²Istituto Nazionale di Fisica Nucleare, Sezione di Roma I, University of Rome "La Sapienza," I-00185 Roma, Italy
⁵³Rutgers University, Piscataway, New Jersey 08855, USA
⁵⁴Texas A&M University, College Station, Texas 77843, USA
⁵⁵Istituto Nazionale di Fisica Nucleare, University of Trieste/Udine, Italy
⁵⁶University of Tsukuba, Tsukuba, Ibaraki 305, Japan
⁵⁷Tufts University, Medford, Massachusetts 02155, USA
⁵⁸Waseda University, Tokyo 169, Japan
⁵⁹Wayne State University, Detroit, Michigan 48201, USA
⁶⁰University of Wisconsin, Madison, Wisconsin 53706, USA
⁶¹Yale University, New Haven, Connecticut 06520, USA
- (Received 10 December 2006; published 29 January 2007)

We present a new measurement of the B^+ meson differential cross section $d\sigma/dp_T$ at $\sqrt{s} = 1960$ GeV. The data correspond to an integrated luminosity of 739 pb^{-1} collected with the upgraded CDF detector (CDF II) at the Fermilab Tevatron collider. B^+ candidates are reconstructed through the decay $B^+ \rightarrow J/\psi K^+$, with $J/\psi \rightarrow \mu^+ \mu^-$. The integrated cross section for producing B^+ mesons with $p_T \geq 6$ GeV/c and $|\eta| \leq 1$ is measured to be $2.78 \pm 0.24 \mu\text{b}$.

DOI: [10.1103/PhysRevD.75.012010](https://doi.org/10.1103/PhysRevD.75.012010)

PACS numbers: 13.85.Ni, 12.38.Qk, 13.25.Hw, 14.40.Nd

- ^aVisiting scientist from University of Athens
^bVisiting scientist from University of Bristol
^cVisiting scientist from University Libre de Bruxelles
^dVisiting scientist from Cornell University
^eVisiting scientist from University of Cyprus
^fVisiting scientist from University of Dublin
^gVisiting scientist from University of Edinburgh
^hVisiting scientist from University of Heidelberg
ⁱVisiting scientist from Universidad Iberoamericana
^jVisiting scientist from University of Manchester
^kVisiting scientist from Nagasaki Institute of Applied Science
^lVisiting scientist from University de Oviedo
^mVisiting scientist from University of London, Queen Mary and Westfield College
ⁿVisiting scientist from Texas Tech University
^oVisiting scientist from IFIC (CSIC-Universitat de Valencia)

I. INTRODUCTION

Measurements of the bottom quark production cross section at the Tevatron collider probe the ability of perturbative QCD to predict absolute rates in hadronic collisions. At the perturbative level, calculations of the hard scattering cross sections have been carried out at next-to-leading order (NLO) [1] and also implemented with logarithmic p_T^b/m_b corrections¹ evaluated to next-to-leading logarithmic accuracy (NLL) [2]. In both cases, these QCD predictions are affected by large theoretical uncertainties such as

¹Mass (m_b) and transverse momentum (p_T^b) of the bottom quarks involved in the hard scattering.

the dependence on the choice of the renormalization and factorization scales and the b -quark mass [3,4]. Accurate measurements could help in improving the theoretical prediction. Unfortunately, as noted in Ref. [5], measurements of the b -quark cross section at the Tevatron appear to be inconsistent among themselves. Reference [5] uses the prediction of a NLO calculation [1] implemented with a nonperturbative model for the b -quark fragmentation² in order to compare all measurements performed at the Tevatron. This calculation predicts $\sigma(p_T^{B^+} \geq 6 \text{ GeV}/c, |y|^{B^+} \leq 1) = 0.9 \mu\text{b}$. Previous measurements [9,10] performed by the CDF collaboration at $\sqrt{s} = 1.8 \text{ TeV}$ yield $\sigma(p_T^{B^+} \geq 6 \text{ GeV}/c, |y|^{B^+} \leq 1) = 2.66 \pm 0.61$ and $3.6 \pm 0.6 \mu\text{b}$, respectively. The ratios of these measurements to the NLO prediction are (2.9 ± 0.7) and (4.0 ± 0.6) , respectively. In contrast, the ratios of the CDF and D0 measurements of the b cross section, that are not based upon the detection of J/ψ mesons [11–15], to the same theoretical prediction have an appreciably smaller average (2.2 with a 0.2 RMS deviation [5]). The cause of the inconsistency could be experimental difficulties inherent to each result or some underlying, and not yet appreciated, production of new physics. Therefore, it is of interest to clarify the experimental situation.

This paper presents a new measurement of the B^+ production cross section that uses fully reconstructed $B^\pm \rightarrow J/\psi K^\pm$ decays. We follow closely the experimental procedure used in Refs. [9,10], but we simplify the analysis selection criteria in order to reduce systematic uncertainties. The B^+ production cross section is the ratio of the number of observed B^+ candidates to the product of the detector acceptance, integrated luminosity, and branching fraction of the decay $B^+ \rightarrow J/\psi K^+$ with $J/\psi \rightarrow \mu^+ \mu^-$. We use B^\pm candidates, and the B^+ cross section is derived assuming charge (C) invariance in the production process. Section II describes the detector systems relevant to this analysis. The data collection, event selection, and B^\pm reconstruction are described in Sec. III. In Sec. IV, we evaluate the detector acceptance and derive the total and differential B^+ cross section. Our conclusions are presented in Sec. V.

II. THE CDF II DETECTOR

CDF is a multipurpose detector, equipped with a charged particle spectrometer and a finely segmented calorimeter. In this section, we describe the detector components that

²This calculation uses a b -quark mass of $m_b = 4.75 \text{ GeV}/c^2$, renormalization and factorization scales $\mu_R = \mu_F = \sqrt{p_T^2 + m_b^2}$, the MRSD₀ [6] fit to the parton distribution functions (PDF), and a fragmentation fraction $f_u = 0.375$. The fragmentation model is based on the Peterson fragmentation function [7] with the ϵ parameter set to 0.006 according to fits to e^+e^- data [8].

are relevant to this analysis. The description of these subsystems can be found in Refs. [16–22]. Two devices inside the 1.4 T solenoid are used for measuring the momentum of charged particles: the silicon vertex detector (SVX II) and the central tracking chamber (COT). The SVX II consists of double-sided microstrip sensors arranged in five cylindrical shells with radii between 2.5 and 10.6 cm. The detector is divided into three contiguous five-layer sections along the beam direction for a total z coverage³ of 90 cm. The COT is a cylindrical drift chamber containing 96 sense wire layers grouped into eight alternating superlayers of axial and stereo wires. Its active volume covers $|z| \leq 155 \text{ cm}$ and 40 to 140 cm in radius. The central muon detector (CMU) is located around the central electromagnetic and hadronic calorimeters, which have a thickness of 5.5 interaction lengths at normal incidence.

The CMU detector covers a nominal pseudorapidity range $|\eta| \leq 0.63$ relative to the center of the detector, and is segmented into two barrels of 24 modules, each covering 15° in ϕ . Every module is further segmented into three submodules, each covering 4.2° in ϕ and consisting of four layers of drift chambers. The smallest drift unit, called a stack, covers a 1.2° angle in ϕ . Adjacent pairs of stacks are combined together into a tower. A track segment (hits in two out of four layers of a stack) detected in a tower is referred to as a CMU stub. A second set of muon drift chambers (CMP) is located behind an additional steel absorber of 3.3 interaction lengths. Muons which produce a stub in both CMU and CMP systems are called CMUP muons.

The luminosity is measured using gaseous Cherenkov counters (CLC) that monitor the rate of inelastic $p\bar{p}$ collisions. The inelastic $p\bar{p}$ cross section at $\sqrt{s} = 1960 \text{ GeV}$ is scaled from measurements at $\sqrt{s} = 1800 \text{ GeV}$ using the calculations in Ref. [23]. The integrated luminosity is determined with a 6% systematic accuracy [24].

CDF uses a three-level trigger system. At Level 1 (L1), data from every beam crossing are stored in a pipeline capable of buffering data from 42 beam crossings. The L1 trigger either rejects events or copies them into one of the four Level 2 (L2) buffers. Events that pass the L1 and L2 selection criteria are sent to the Level 3 (L3) trigger, a cluster of computers running speed-optimized reconstruction code.

For this study, we select events with two muon candidates identified by the L1 and L2 triggers. The L1 trigger uses tracks with $p_T \geq 1.5 \text{ GeV}/c$ found by a fast track processor (XFT). The XFT examines COT hits from four

³In the CDF coordinate system, θ and ϕ are the polar and azimuthal angles of a track, respectively, defined with respect to the proton beam direction, z . The pseudorapidity η is defined as $-\log \tan(\theta/2)$. The transverse momentum of a particle is $p_T = P \sin(\theta)$. The rapidity is defined as $y = 1/2 \cdot \log((E + p_z)/(E - p_z))$, where E and p_z are the energy and longitudinal momentum of the particle associated with the track.

axial superlayers and provides $r - \phi$ information. The XFT finds tracks with $p_T \geq 1.5$ GeV/ c in azimuthal sections of 1.25° . The XFT passes the tracks to a set of extrapolation units that determines the CMU towers in which a CMU stub should be found if the track is a muon. If a stub is found, a L1 CMU primitive is generated. The L1 dimuon trigger requires at least two CMU primitives, separated by at least two CMU towers. At L1, there is no requirement that muons have opposite charge. During the data-taking period in which the dimuon sample used for this analysis was collected, the Tevatron luminosity has increased from 1 to 100×10^{30} cm $^{-2}$ s $^{-1}$. Accordingly, the L2 trigger, that started with no additional requirement, has incrementally required dimuons with opposite charge, opening azimuthal angle $\delta\phi \leq 120^\circ$, and single muons with $p_T \geq 2$ GeV/ c . All these trigger requirements are mimicked by the detector simulation on a run-by-run basis. At L3, muons are required to have opposite charge, invariant mass in the window 2.7–4.0 GeV/ c^2 , and $|\delta z_0| \leq 5$ cm, where z_0 is the z coordinate of the muon track at its point of closest approach to the beam line in the $r - \phi$ plane. These requirements define the $J/\psi \rightarrow \mu^+ \mu^-$ trigger.

We use two additional triggers in order to verify the detector simulation. The first trigger (CMUP p_T4) selects events with at least one L1 and one L2 CMUP primitive with $p_T \geq 4$ GeV/ c , and an additional muon found by the L3 algorithms. Events collected with this trigger are used to measure the muon trigger efficiency. The second trigger (μ -SVT) requires a L1 CMUP primitive with $p_T \geq 4$ GeV/ c accompanied by a L2 requirement of an additional XFT track with $p_T \geq 2$ GeV/ c and displaced from the interaction point. These events are used to verify the muon detector acceptance and the muon reconstruction efficiency.

III. DATA SELECTION AND B^\pm RECONSTRUCTION

We search for $B^\pm \rightarrow J/\psi K^\pm$ candidates in the data set selected by the $J/\psi \rightarrow \mu^+ \mu^-$ trigger. Events are reconstructed offline taking advantage of more refined calibration constants and reconstruction algorithms.

The transverse momentum resolution of tracks reconstructed using COT hits is $\sigma(p_T)/p_T^2 \approx 0.0017$ [GeV/ c] $^{-1}$. COT tracks are extrapolated into the SVX II detector and refitted adding hits consistent with the track extrapolation. Stubs reconstructed in the CMU detector are matched to tracks with $p_T \geq 1.3$ GeV/ c . A track is identified as a CMU muon if $\Delta r\phi$, the distance in the $r - \phi$ plane between the track projected to the CMU chambers and a CMU stub, is less than 30 cm. We also require that muon-candidate stubs correspond to a L1 CMU primitive, and correct the muon momentum for energy losses in the detector.

We search for J/ψ candidates by using pairs of CMU muons with opposite charge, and $p_T \geq 2$ GeV/ c (this requirement for each muon track avoids the region of rapidly changing efficiency around the trigger threshold). The invariant mass of a muon pair is evaluated by constraining the two muon tracks to originate from a common point in three-dimensional space (vertex constraint) in order to improve the mass resolution. All muon pairs with invariant mass in the range 3.05–3.15 GeV/ c^2 are considered to be J/ψ candidates.

If a J/ψ candidate is found, we search for B^\pm mesons by considering all remaining charged particle tracks in the event as possible kaon candidates. As in previous measurements [9,10], we select tracks with $p_T \geq 1.25$ GeV/ c and with $|\delta z_0| \leq 1.5$ cm with respect to the z_0 position of the J/ψ candidate. We require that kaon-candidate tracks have at least 10 hits in both COT axial and stereo superlayers. This limits the pseudorapidity acceptance to $|\eta| \leq 1.3$. The invariant mass of the $\mu^+ \mu^- K^\pm$ system is evaluated constraining the corresponding tracks to have a common origin while the $\mu^+ \mu^-$ invariant mass is constrained to the value of 3.0969 GeV/ c^2 [25]. As in Refs. [9,10], we select B^\pm candidates with $p_T \geq 6$ GeV/ c . From the pseudorapidity acceptance of CMU muons ($|\eta| \leq 0.8$) and the p_T cuts on the μ^\pm and B^\pm transverse momenta, it follows that: (i) no kaon from B^\pm decays is emitted at $|\eta| \geq 1.3$; (ii) the reconstructed B^\pm candidates have rapidity $|y| \leq 1$.

In contrast with the analyses in Refs. [9,10], we do not require the proper decay length of the B^\pm candidates to be larger than 100 μ m. By doing so, we avoid two large sources of systematic uncertainty: (i) the simulated effi-

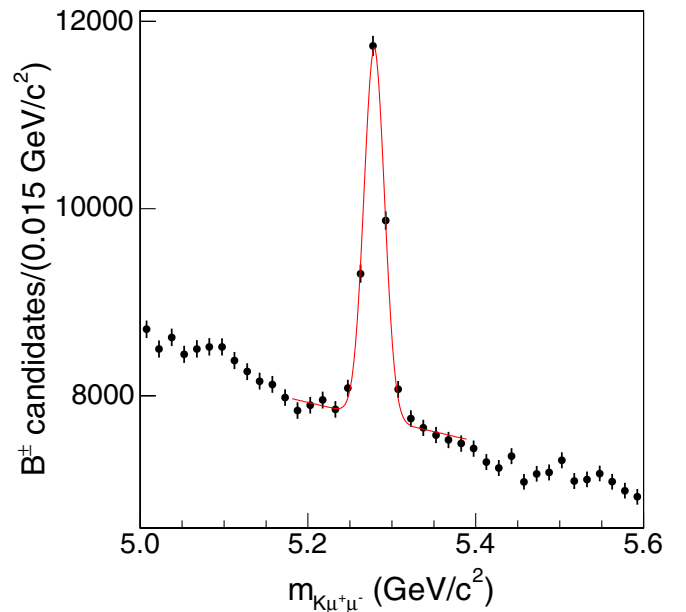


FIG. 1 (color online). Invariant mass distribution of all B^\pm candidates. The line represents a fit to the data using a first order polynomial plus a Gaussian function in order to estimate the background and the B^\pm signal, respectively.

ciency of the SVX II detector; (ii) the dependence of the decay length distribution on the simulated SVX II resolution and B^\pm transverse momentum distribution. The invariant mass distribution of all B^\pm candidates found in this study is shown in Fig. 1.

IV. DIFFERENTIAL CROSS SECTION

To measure the differential cross section, we divide the sample of B^\pm candidates into five p_T bins: 6–9, 9–12, 12–15, 15–25, and ≥ 25 GeV/ c [9,10]. In each p_T bin, we fit the invariant mass distribution of the B^\pm candidates with a binned maximum-likelihood method to determine the number of B^\pm mesons. The fit likelihood uses a Gaussian function to model the B^\pm signal. The background under the B^\pm signal arises from combinations of J/ψ mesons, 80% of which do not originate from B^\pm decays [26], with random tracks. Combinations of J/ψ mesons with a track produced by the same B -hadron $\rightarrow J/\psi + \geq 2$ prong decay (partially reconstructed B^\pm meson) populate the mass region below 5.16 GeV/ c^2 . As in previous measurements [9,10], we use a first order polynomial to estimate the underlying combinatorial background (as shown by Fig. 1, the combinatorial background in the mass region above the B^\pm meson signal is quite well modeled by a straight line). We fit the data in the invariant mass range 5.18–5.39 GeV/ c^2 . The lower limit is chosen to avoid the region populated by partially reconstructed B -hadron decays. The width of the fitted mass range determines the statistical error of the background estimate. Since we have a much larger data set than previous measurements [9,10], we can afford to fit the data in a smaller mass range in order to reduce the systematic uncertainty due to the background modeling.

The average of the B^\pm mass values returned by the fits in the different p_T bins is 5.2790 GeV/ c^2 with a 0.5 MeV/ c^2 RMS deviation, in agreement with the PDG value [25]. In the fit used to determine the number of B^\pm mesons, we fix the B^\pm mass value to 5.279 GeV/ c^2 [25]. The width of the Gaussian is a free fit parameter; the value of σ returned by the fit increases from 12.0 ± 0.4 to 20.0 ± 0.4 MeV/ c^2 from the first to last p_T bin, in agreement with the simulation prediction. The fits are shown in Figs. 2–6. They return a signal of 2792 ± 186 , 2373 ± 110 , 1365 ± 66 , 1390 ± 63 , and 277 ± 44 B^\pm mesons in the five p_T bins.

We have investigated possible systematic uncertainties in the fit results. We have studied the contribution of the $B \rightarrow J/\psi\pi$ decay mode, the branching fraction of which is $(4.9 \pm 0.6)\%$ of that of the $B \rightarrow J/\psi K$ decay mode [25]. As shown in Ref. [27], the invariant mass distribution of these Cabibbo-suppressed B decays, reconstructed assuming that pions are kaons, is shifted into the mass region 5.28–5.44 GeV/ c^2 , which partially overlaps with that of the $B \rightarrow J/\psi K$ decay mode. However, part of this Cabibbo-suppressed contribution is also used by the fit to predict the background under the $B \rightarrow J/\psi K$ signal with

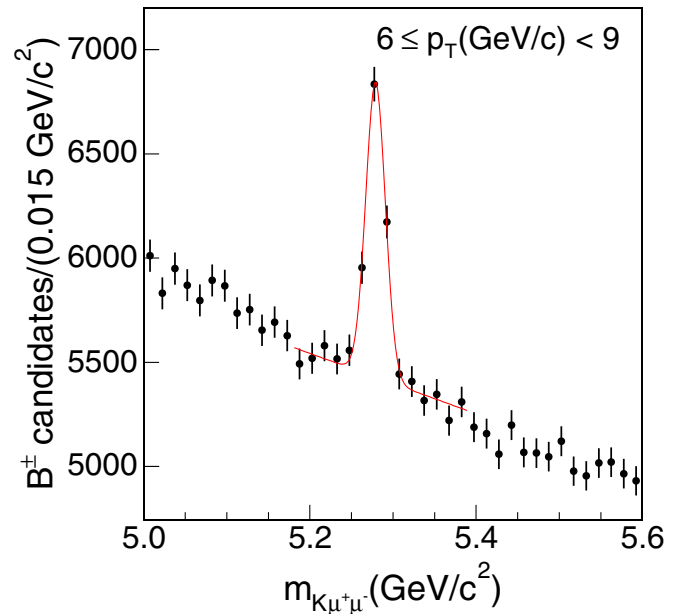


FIG. 2 (color online). Invariant mass distribution of B^\pm candidates with $6 \leq p_T \leq 9$ GeV/ c . The line represents the best fit to the data described in the text.

the effect of reducing its size. When adding the expected contribution of these Cabibbo-suppressed decays, the $B \rightarrow J/\psi K$ signal returned by the fit decreases by $(1 \pm 1)\%$ (we do not apply the 1% correction to the final result, but the uncertainty of the correction is included in the systematic error). We have investigated other possible causes of systematic uncertainties in the B signal estimate. We have

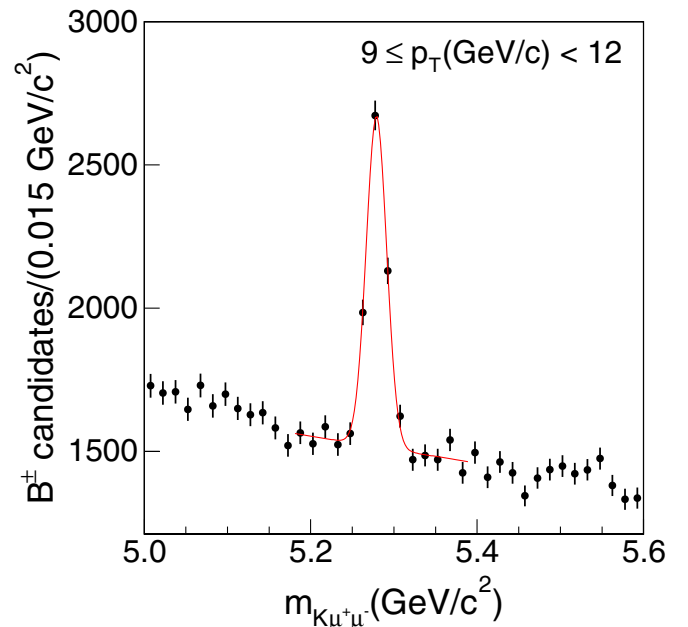


FIG. 3 (color online). Invariant mass distribution of B^\pm candidates with $9 \leq p_T \leq 12$ GeV/ c . The line represents the best fit to the data described in the text.

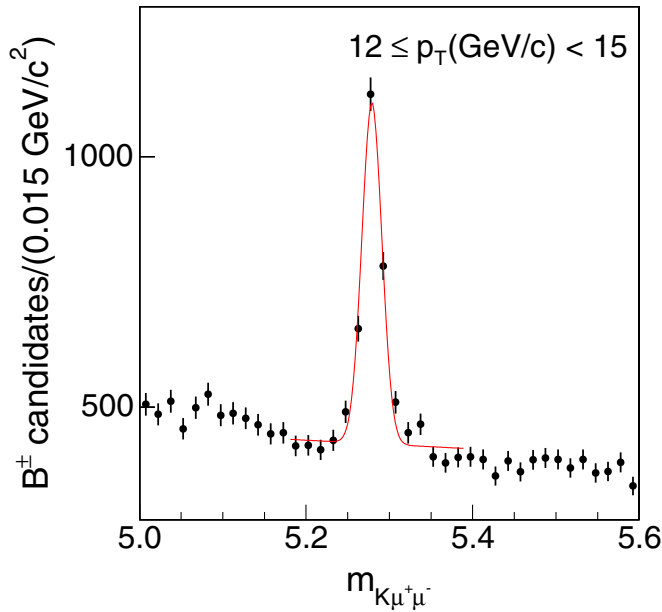


FIG. 4 (color online). Invariant mass distribution of B^\pm candidates with $12 \leq p_T \leq 15$ GeV/c. The line represents the best fit to the data described in the text.

compared the results of our fit with those returned using an unbinned likelihood method. We have decreased the fitted mass range to 5.24–5.33 GeV/ c^2 , and we have fitted the larger mass interval 5.18–5.60 GeV/ c^2 . We have fitted the signal with two Gaussian functions in order to study detector resolution effects. The B signal returned by these fits does not vary by more than $\pm 1.5\%$. Therefore, we attribute an overall $\pm 2\%$ systematic uncertainty to the fit results.

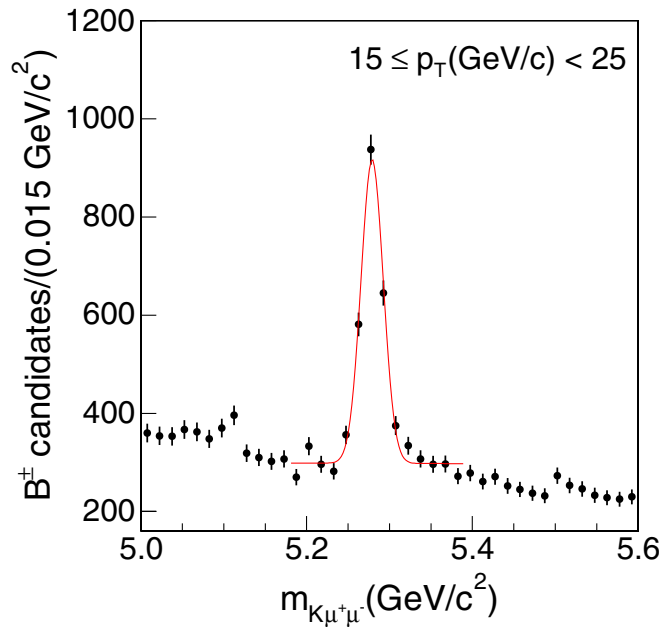


FIG. 5 (color online). Invariant mass distribution of B^\pm candidates with $15 \leq p_T \leq 25$ GeV/c. The line represents the best fit to the data described in the text.

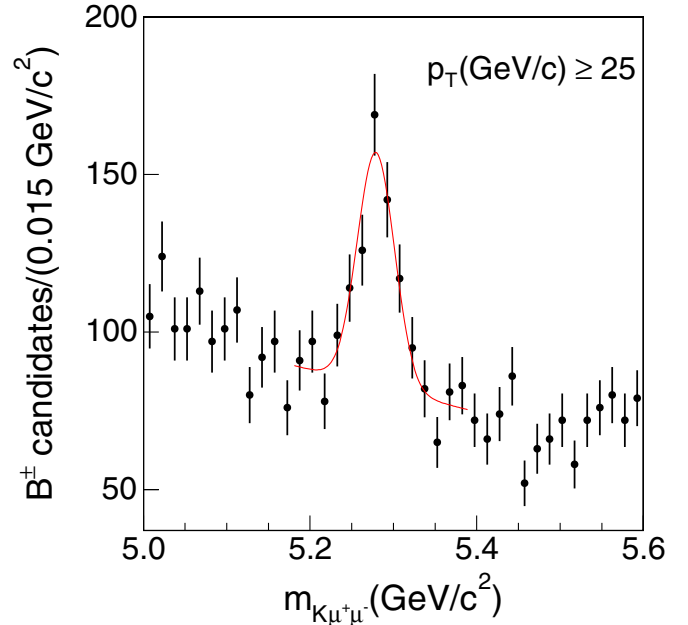


FIG. 6 (color online). Invariant mass distribution of B^\pm candidates with $p_T \geq 25$ GeV/c. The line represents the best fit to the data described in the text.

A. Acceptances and efficiencies

The detector acceptance is calculated with a Monte Carlo simulation based upon a NLO calculation². The B^\pm decay is modeled with the EVTGEN Monte Carlo program [28] that accounts for the J/ψ longitudinal polarization [29]. The detector response to particles produced by B^\pm decays is modeled with the CDF II detector simulation that in turn is based on the GEANT Monte Carlo program [30]. The simulation includes the generation of L1 CMU trigger primitives. Simulated events are processed and selected with the same analysis code used for the data. The acceptances estimated using the simulation are listed in Table I. We use the data to verify the detector acceptance and efficiencies evaluated using the CDF II detector simulation. We adjust the simulation to match measurements in the data of: (i) the offline COT track reconstruction efficiency; (ii) the CMU detector acceptance and efficiency;

TABLE I. Detector acceptance, \mathcal{A} , as a function of the B^\pm p_T . The acceptance $\mathcal{A}_{\text{corr}}$ includes corrections evaluated using the data. The average $\langle p_T \rangle$ is the value at which the theoretical differential cross section [1] equals the integrated cross section in each momentum bin divided by the bin width.

p_T range (GeV/c)	$\langle p_T \rangle$ (GeV/c)	\mathcal{A} (%)	$\mathcal{A}_{\text{corr}}$ (%)
6–9	7.37	1.545	1.780 ± 0.045
9–12	10.38	3.824	4.405 ± 0.111
12–15	13.39	5.966	6.872 ± 0.173
15–25	19.10	8.819	10.16 ± 0.25
≥ 25		12.516	14.42 ± 0.36

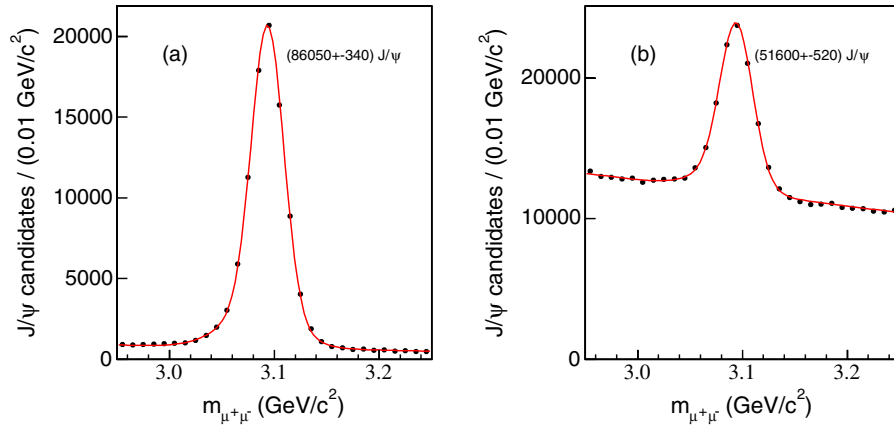


FIG. 7 (color online). Invariant mass distribution of a CMUP muon paired with all charged tracks in the event with (a) or without (b) a CMU stub. Lines represent the fits described in the text.

(iii) the efficiency for finding L1 CMU primitives; and (iv) the efficiency of the L1, L2, and L3 triggers.

In the simulation, the offline COT track reconstruction efficiency is given by the fraction of tracks, which at generator level satisfy the p_T and η selection cuts, that survive after selecting fully simulated events as the data. The COT track reconstruction efficiency is found to be 0.998 ± 0.002 . The same efficiency in the data is measured by embedding COT hits generated from simulated tracks into J/ψ data. In Ref. [26], the COT track reconstruction efficiency in the data is measured to be 0.996 with a ≈ 0.006 systematic accuracy.⁴ We conclude that the efficiencies for reconstructing the $\mu^+ \mu^- K^\pm$ system in the data and the simulation are equal within a 2% systematic error. Kaon decay and interactions are modeled with the CDF II detector simulation. Because of the uncertainties of the detector materials and the nuclear interaction cross sections, the kaon tracking efficiency has an additional 0.3% uncertainty [32].

In the simulation, the fraction of CMU stubs generated by muon tracks with $p_T \geq 2$ GeV/ c and $|\eta| \leq 0.8$ is 0.6439 ± 0.0004 . In the data, this efficiency is measured by using $J/\psi \rightarrow \mu^+ \mu^-$ decays acquired with the μ -SVT trigger. We evaluate the invariant mass of all pairs of a CMUP track and a track with displaced impact parameter, $p_T \geq 2$ GeV/ c , and $|\eta| \leq 0.8$. We fit the invariant mass distribution with a first order polynomial plus two Gaussian functions to extract the J/ψ signal. From the number of J/ψ mesons reconstructed using displaced tracks with or without a CMU stub (Fig. 7(a) and 7(b), respectively), we derive an efficiency of 0.6251 ± 0.0047 . The integrated efficiency is evaluated after having weighted the p_T and η distributions of displaced tracks

⁴The efficiency measurement was performed in a subset of the data used for this analysis. Studies of independent data samples collected in the data-taking period used for this analysis show that changes of the track reconstruction efficiency are appreciably smaller than the quoted systematic uncertainty [31].

in the data to be equal to those of muons from B decays in the simulation.

In the simulation, the efficiency for finding a CMU primitive (CMU stub matched by a XFT track) is 0.8369 ± 0.0004 . This efficiency is measured in the data by using events acquired with the CMUP_{p_T4} trigger. We combine the CMUP muon with all other CMU muons found in the event with and without a L1 CMU primitive. We extract the number of $J/\psi \rightarrow \mu^+ \mu^-$ mesons by fitting the invariant mass distributions of all candidates with a first order polynomial plus two Gaussian functions. By comparing the fitted numbers of J/ψ candidates with and without L1 CMU primitive (Fig. 8(a) and 8(b), respectively) we derive an efficiency of 0.9276 ± 0.0005 . The integrated efficiency is evaluated after having weighted the p_T and η distributions of the additional CMU muons to be equal to that of muons from B decays in the simulation.

In the simulation, the efficiencies of the L1 and L2 triggers are 0.9868 and 0.9939, respectively. By studying J/ψ candidates acquired with the CMUP_{p_T4} trigger, the L1 efficiency is measured to be 0.9879 ± 0.0009 , and that of the L2 trigger 0.9948 ± 0.0001 . The L3 trigger is not simulated. The L3 trigger efficiency is dominated by differences between the online and offline reconstruction code efficiency.⁵ The relative L3 efficiency for reconstructing a single muon identified by the offline code has been measured to be 0.997 ± 0.002 [26]. The reconstruction efficiencies in the data and in the simulation are summarized in Table II.

B. Results

The differential cross section $d\sigma/dp_T$ is calculated as

$$\frac{d\sigma(B^+)}{dp_T} = \frac{N/2}{\Delta p_T \times \mathcal{L} \times \mathcal{A}_{\text{corr}} \times BR} \quad (1)$$

⁵Online algorithms are faster but less accurate than the offline reconstruction code.

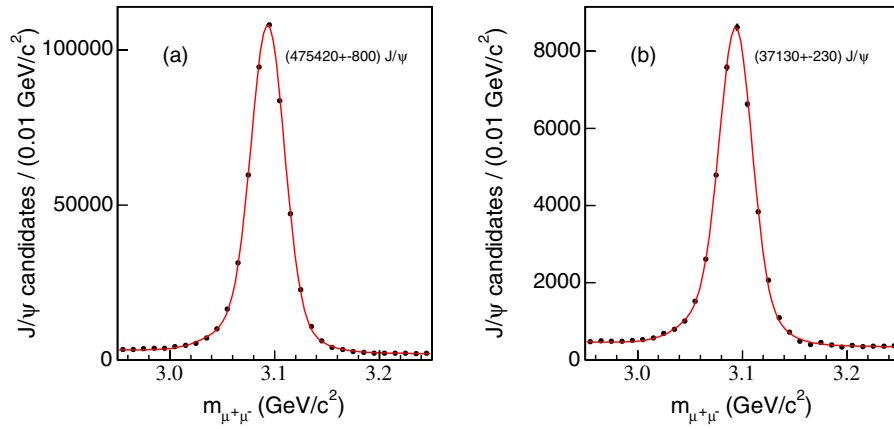


FIG. 8 (color online). Invariant mass distribution of a CMUP muon paired with all CMU muons in the event with (a) or without (b) a L1 CMU primitive. Lines represent the fits described in the text.

TABLE II. Summary of efficiencies for reconstructing B^\pm candidates in the data and the simulation. The last column indicates the corrections applied to the simulated acceptance and used to derive $\mathcal{A}_{\text{corr}}$ in Table I.

Source	Data	Simulation	Corr.
COT tracking	$(0.996 \pm 0.006)^3$	$(0.998 \pm 0.002)^3$	1.00 ± 0.02
Kaon interaction			1.000 ± 0.003
CMU acc. and eff.	$(0.6251 \pm 0.0047)^2$	$(0.6439 \pm 0.0004)^2$	0.942 ± 0.014
L1 CMU primitives	$(0.9276 \pm 0.0005)^2$	$(0.8369 \pm 0.0004)^2$	1.228 ± 0.002
L1 eff.	0.9879 ± 0.0009	0.9868	1.0011 ± 0.0009
L2 eff.	0.9948 ± 0.0001	0.9939	1.0009 ± 0.0001
L3 eff.	$(0.997 \pm 0.002)^2$	1	0.994 ± 0.004
Total	0.328 ± 0.008	0.283 ± 0.002	1.152 ± 0.029

where N is the number of B^\pm mesons determined from the likelihood fit to the invariant mass distribution of the $J/\psi K^\pm$ candidates in each p_T bin. The factor 1/2 accounts for the fact that both B^+ and B^- mesons are used and assumes C invariance at production. The bin width Δp_T and $\mathcal{A}_{\text{corr}}$, the geometric and kinematic acceptance that includes trigger and tracking efficiencies measured with the data, are listed in Table I. The integrated luminosity of the data set is $\mathcal{L} = 739 \pm 44 \text{ pb}^{-1}$. The branching ratio $\text{BR} = (5.98 \pm 0.22) \times 10^{-5}$ is derived from the branching

fractions $\text{BR}(B^\pm \rightarrow J/\psi K^\pm) = (1.008 \pm 0.035) \times 10^{-3}$ and $\text{BR}(J/\psi \rightarrow \mu^+ \mu^-) = (5.93 \pm 0.06) \times 10^{-2}$ [25].

The measured B^+ differential cross section as a function of its transverse momentum is listed in Table III. The integrated cross section is

$$\sigma_{B^+}(p_T \geq 6.0 \text{ GeV}/c, |y| < 1) = 2.78 \pm 0.24 \text{ } \mu\text{b}, \quad (2)$$

where the 8.8% error is the sum in quadrature of the 6% error on the integrated luminosity, the 3.6% uncertainty of the $B^+ \rightarrow J/\psi K^+$ and $J/\psi \rightarrow \mu^+ \mu^-$ branching fractions,

TABLE III. Observed differential cross section, $d\sigma/dp_T$ (nb/GeV/c), for B^+ mesons with rapidity $|y| \leq 1$. Errors are the sum in quadrature of statistical errors (shown in parentheses) and systematic uncertainties due to luminosity (6%), branching ratios (3.6%), acceptance (2.5%), and fitting procedure (2.0%). The relative systematic uncertainties are the same in each p_T bin. The integrated cross section for $p_T \geq 25 \text{ GeV}/c$ is $21.7 \pm 3.7 \text{ nb}$.

$\langle p_T \rangle$ (GeV/c)	Events	Acceptance (%)	$d\sigma/dp_T$
7.38	2792 ± 186	1.780 ± 0.045	591.7 ± 59.0 (39.3 stat.)
10.38	2373 ± 110	4.405 ± 0.111	203.2 ± 17.8 (9.4 stat.)
13.39	1365 ± 66	6.872 ± 0.173	74.9 ± 6.6 (3.6 stat.)
19.10	1390 ± 63	10.16 ± 0.25	15.5 ± 1.3 (0.7 stat.)
≥ 25	277 ± 44	14.42 ± 0.36	

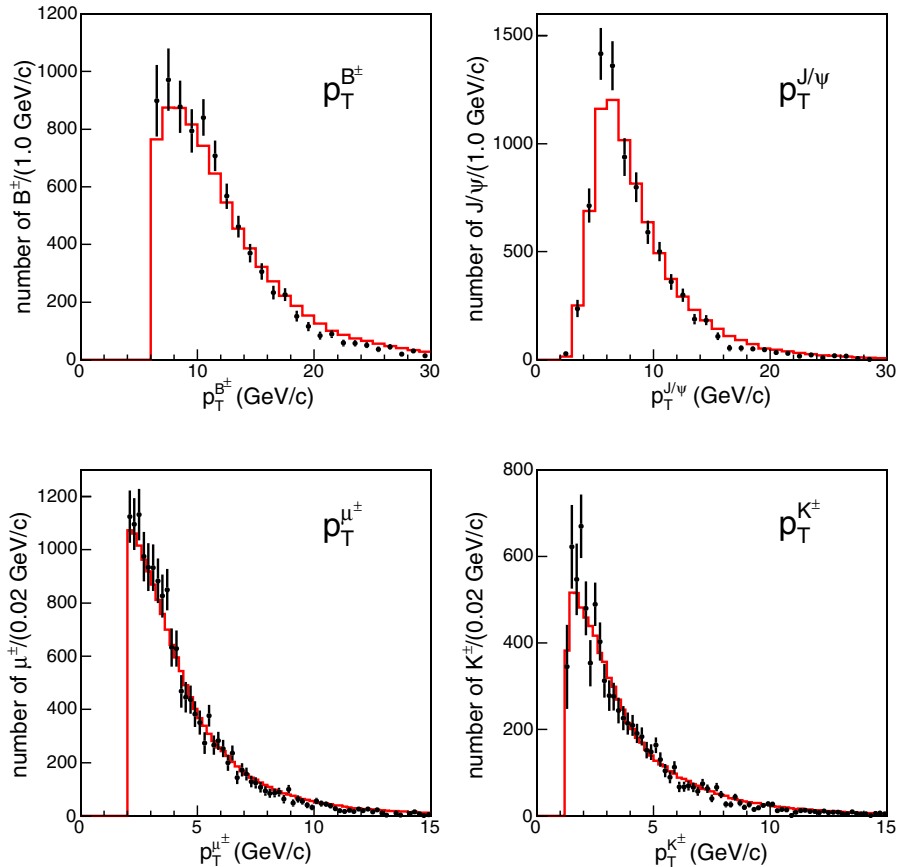


FIG. 9 (color online). Transverse momentum distributions in the data (\bullet) and simulation (solid histogram). The simulation is normalized to the $B^\pm \rightarrow \mu^+ \mu^- K^\pm$ signal observed in the data (see text).

the 2.5% uncertainty of the acceptance calculation, the 2% systematic uncertainty of the fit, and the 4.4% statistical error.

For completeness, Fig. 9 compares transverse momentum distributions in the data and in the simulation, based on the NLO QCD prediction², that has been used to evaluate the detector acceptance. Figure 10 compares B^\pm meson rapidity distributions. Data and simulation are normalized to the same number of events. Each distribution is constructed using $J/\psi K^\pm$ candidates with invariant mass in the range 5.255–5.315 GeV/c^2 (region #1). The background contribution is subtracted using candidates in the mass range 5.18–5.24 and 5.33–5.425 GeV/c^2 . The background normalization is the number of events in region #1 minus the number of B^\pm candidates determined by the fit listed in Table III. One notes the fair agreement between data and untuned QCD prediction.⁶

⁶The p_T distributions of the B^\pm and J/ψ mesons in the data are slightly softer than those of the simulation; this difference is not relevant for the result of the study because the B^\pm kinematic acceptance has been evaluated for each p_T^B bin and the calibration of the simulated acceptance using the data do not depend on the muon and kaon transverse momenta.

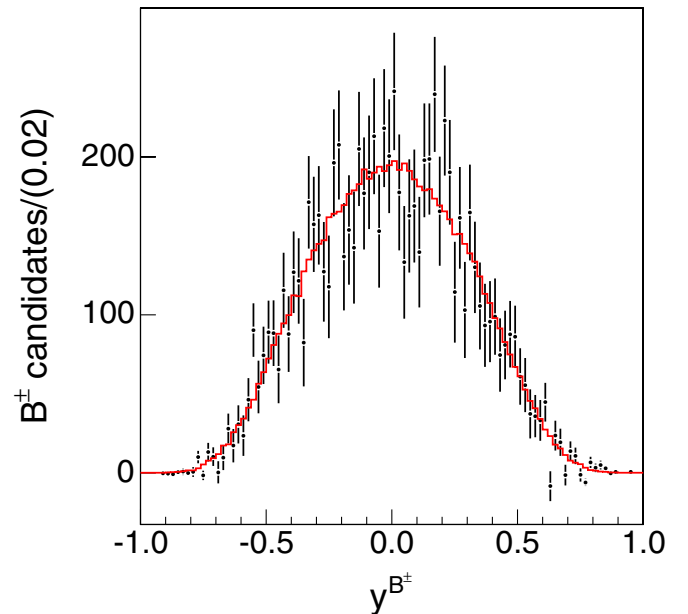


FIG. 10 (color online). Rapidity distributions of B^\pm mesons in the data (\bullet) and simulation (solid histogram). The simulation is normalized to the $B^\pm \rightarrow \mu^+ \mu^- K^\pm$ signal observed in the data (see text).

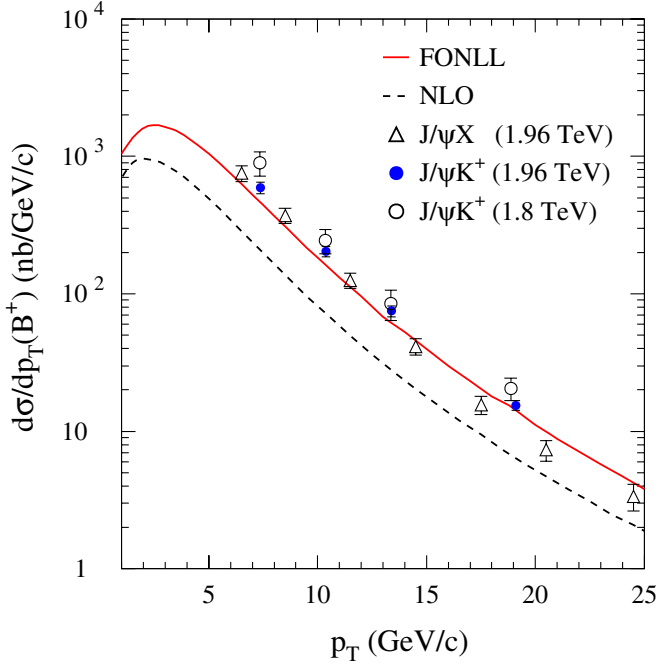


FIG. 11 (color online). Measurements of the B^+ differential cross section ($|y^{B^+}| \leq 1$) at the Tevatron are compared to NLO and FONLL theoretical predictions. The FONLL result utilizes the CTEQ6M fits to the parton distribution functions, and nonperturbative fragmentation functions consistent with the accuracy level of the calculation [36]. The NLO prediction, used to evaluate the kinematical acceptance of this experiment and to compare different measurements of the b quark cross section at the Tevatron in Ref. [5], uses the MRSD₀ [6] fits and the Peterson fragmentation model with $\epsilon = 0.006$ (see text). The result of this experiment (\bullet) is shown together with those of (Δ) Ref. [26] and (\circ) Ref. [9]; the result of Ref. [9] has been increased by 10% to account for the expected increase of the cross section from $\sqrt{s} = 1.8$ to 1.96 TeV [1]. For each experiment, errors are the sum in quadrature of statistical and systematic uncertainties.

V. CONCLUSIONS

We use the exclusive decay $B^\pm \rightarrow J/\psi K^\pm$ to measure the B^+ production cross section in $p\bar{p}$ collisions at $\sqrt{s} = 1960$ GeV. The measurement is based on a sample of 8197 ± 239 B^\pm mesons selected from 739 pb^{-1} of data collected with the CDF II detector at the Fermilab Tevatron collider. The B^+ production cross section is measured to be

$$\sigma_{B^+}(p_T \geq 6.0 \text{ GeV}/c, |y| < 1) = (2.78 \pm 0.24) \mu\text{b}.$$

To compare with other Tevatron measurements, we choose as a theoretical benchmark the NLO QCD predic-

tion [1] that uses a b -quark mass of $m_b = 4.75 \text{ GeV}/c^2$, renormalization and factorization scales $\mu_R = \mu_F = \sqrt{p_T^2 + m_b^2}$, the MRSD₀ [6] fit to the parton distribution functions (PDF), a fragmentation fraction $f_u = 0.375$, and a fragmentation model based on the Peterson fragmentation function with the ϵ parameter set to 0.006. The ratio of the present measurement to this theoretical prediction is 2.80 ± 0.24 . Previous measurements of the single b -quark cross section based on the detection of J/ψ mesons yield the following ratios to the same theoretical prediction: 2.90 ± 0.67 [9], 4.0 ± 0.6 [10], 4.0 ± 0.4 [33], and 3.14 ± 0.28 [26]. In contrast, all CDF and D0 measurements of the single b production cross section that are based upon detection of a lepton from b -quark decays [11–15] yield a smaller average ratio to the same theoretical prediction (2.2 with a 0.2 RMS deviation [5]). As shown in Fig. 11, our measurement agrees with the value inferred from the J/ψ inclusive cross section [26] [$\sigma_{B^+}(p_T \geq 6.0 \text{ GeV}/c, |y| < 1) = 2.4 \pm 0.4 \mu\text{b}$] and is within the range of values predicted by the FONLL calculation [2,34] that uses $f_u = 0.389$ [25], the CTEQ6M fits to the parton distribution functions [35], and nonperturbative fragmentation functions consistent with the accuracy level of the QCD calculation [36] ($2.1 \mu\text{b}$ with a $\approx 30\%$ theoretical uncertainty [4]).

ACKNOWLEDGMENTS

We thank the Fermilab staff and the technical staffs of the participating institutions for their vital contributions. This work was supported by the U.S. Department of Energy and National Science Foundation; the Italian Istituto Nazionale di Fisica Nucleare; the Ministry of Education, Culture, Sports, Science and Technology of Japan; the Natural Sciences and Engineering Research Council of Canada; the National Science Council of the Republic of China; the Swiss National Science Foundation; the A.P. Sloan Foundation; the Bundesministerium für Bildung und Forschung, Germany; the Korean Science and Engineering Foundation and the Korean Research Foundation; the Particle Physics and Astronomy Research Council and the Royal Society, UK; the Institut National de Physique Nucleaire et Physique des Particules/CNRS; the Russian Foundation for Basic Research; the Comisión Interministerial de Ciencia y Tecnología, Spain; the European Community's Human Potential Programme under contract No. HPRN-CT-2002-00292; and the Academy of Finland.

- [1] P. Nason, S. Dawson, and R. K. Ellis, Nucl. Phys. **B327**, 49 (1989); P. Nason, S. Dawson, R. K. Ellis *ibid.* **B335**, 260 (1990); W. Beenakker *et al.*, Nucl. Phys. **B351**, 507 (1991).
- [2] M. Cacciari *et al.*, J. High Energy Phys. 05 (1998) 007.
- [3] S. Frixione *et al.*, Adv. Ser. Direct. High Energy Phys. **15**, 609 (1998).
- [4] M. Cacciari *et al.*, J. High Energy Phys. 07 (2004) 033.
- [5] F. Happacher *et al.*, Phys. Rev. D **73**, 014026 (2006); F. Happacher, Status of the Observed and Predicted $b\bar{b}$ Cross Section at the Tevatron, www-conf.kek.jp/dis06/doc/WG5/hfl20-happacher.ps, in Proceedings of DIS 2006, Tsukuba, Japan (unpublished).
- [6] A. D. Martin, W. J. Stirling, and R. G. Roberts, Phys. Rev. D **47**, 867 (1993).
- [7] C. Peterson *et al.*, Phys. Rev. D **27**, 105 (1983).
- [8] J. Chrin, Z. Phys. C **36**, 163 (1987).
- [9] F. Abe *et al.*, Phys. Rev. Lett. **75**, 1451 (1995).
- [10] D. Acosta *et al.*, Phys. Rev. D **65**, 052005 (2002).
- [11] F. Abe *et al.*, Phys. Rev. Lett. **71**, 2396 (1993).
- [12] F. Abe *et al.*, Phys. Rev. Lett. **71**, 500 (1993).
- [13] S. Abachi *et al.*, Phys. Rev. Lett. **74**, 3548 (1995).
- [14] B. Abbott *et al.*, Phys. Lett. B **487**, 264 (2000).
- [15] B. Abbott *et al.*, Phys. Rev. Lett. **85**, 5068 (2000).
- [16] F. Abe *et al.*, Nucl. Instrum. Methods Phys. Res., Sect. A **271**, 387 (1988).
- [17] R. Blair *et al.*, Fermilab Report No. FERMILAB-Pub-96/390-E, 1996 (unpublished).
- [18] A. Sill *et al.*, Nucl. Instrum. Methods Phys. Res., Sect. A **447**, 1 (2000).
- [19] T. Affolder *et al.*, Nucl. Instrum. Methods Phys. Res., Sect. A **526**, 249 (2004).
- [20] G. Ascoli *et al.*, Nucl. Instrum. Methods Phys. Res., Sect. A **268**, 33 (1988).
- [21] J. Elias *et al.*, Nucl. Instrum. Methods Phys. Res., Sect. A **441**, 366 (2000).
- [22] D. Acosta *et al.*, Nucl. Instrum. Methods Phys. Res., Sect. A **461**, 540 (2001).
- [23] M. M. Block and R. N. Cahn, Rev. Mod. Phys. **57**, 563 (1985).
- [24] S. Klimenko *et al.*, Fermilab Report No. FERMILAB-FN-0741, 2003 (unpublished).
- [25] W. M. Yao *et al.*, J. Phys. Lett. **633**, 1 (2006).
- [26] D. Acosta *et al.*, Phys. Rev. D **71**, 032001 (2005).
- [27] A. Abulencia *et al.*, Phys. Rev. D. (to be published).
- [28] D. J. Lange, Nucl. Instrum. Methods Phys. Res., Sect. A **462**, 152 (2001).
- [29] B. Aubert *et al.*, Phys. Rev. D **65**, 032001 (2002).
- [30] R. Brun *et al.*, CERN Report No. CERN-DD-78-2-REV (unpublished); CERN Programming Library Long Write-up Report No. W5013 1993 (unpublished).
- [31] A. Abulencia *et al.*, Phys. Rev. Lett. **95**, 252001 (2005).
- [32] D. Acosta *et al.*, Phys. Rev. Lett. **94**, 122001 (2005).
- [33] F. Abe *et al.*, Phys. Rev. Lett. **79**, 572 (1997).
- [34] M. Cacciari and P. Nason, Phys. Rev. Lett. **89**, 122003 (2002).
- [35] J. Pumplin *et al.*, J. High Energy Phys. 07 (2002) 012.
- [36] P. Nason and C. Oleari, Nucl. Phys. **B565**, 245 (2000); B. Mele and P. Nason, Nucl. Phys. **B361**, 626 (1991); G. Colangelo and P. Nason, Phys. Lett. B **285**, 167 (1992).